

# Hybrid MD-Nernst Planck model of $\alpha$ -hemolysin conductance properties

IOANA COZMUTA<sup>†</sup>, JAMES T. O'KEEFE<sup>‡</sup>, DEEPAK BOSE<sup>†</sup> and VIKTOR STOLC<sup>‡\*</sup>

<sup>†</sup>Eloret<sup>¶</sup> Corporation, NASA Ames Research Center, Moffett Field, CA 94035, USA

<sup>‡</sup>NASA AMES Research Center, Mail Stop 239-11, Moffett Field, CA 94035, USA

(Received March 2004; in final form June 2004)

Motivated by experiments in which an applied electric field translocates polynucleotides through an  $\alpha$ -hemolysin protein channel causing ionic current transient blockade, a hybrid simulation model is proposed to predict the conductance properties of the open channel. Time scales corresponding to ion permeation processes are reached using the Poisson–Nernst–Planck (PNP) electro-diffusion model in which both solvent and local ion concentrations are represented as a continuum. The diffusion coefficients of the ions ( $K^+$  and  $Cl^-$ ) input in the PNP model are, however, calculated from all-atom molecular dynamics (MD). In the MD simulations, a reduced representation of the channel is used. The channel is solvated in a 1 M KCl solution, and an external electric field is applied. The pore specific diffusion coefficients for both ionic species are reduced 5–7 times in comparison to bulk values. Significant statistical variations (17–45%) of the standard deviations of the pore-ions diffusivities are observed. Within the statistics, the ionic diffusivities remain invariable for a range of external applied voltages between 30 and 240 mV. In the 2D-PNP calculations, the pore stem is approximated by a smooth cylinder of radius  $\sim 9$  Å with two constriction blocks where the radius is reduced to  $\sim 6$  Å. The electrostatic potential includes the contribution from the atomistic charges. The MD-PNP model shows that the fixed charges are responsible for both the rectifying behavior of the channel. The atomic charges are also responsible for the slight anion selectivity of the  $\alpha$ -hemolysin pore. Independent of the hierarchy between the anion and cation diffusivities, the anionic contribution to the total ionic current will dominate. The predictions of the MD-PNP model are in good agreement with experimental data and give confidence in the present approach of bridging time scales by combining a microscopic and macroscopic model.

**Keywords:** Ionic current;  $\alpha$ -Hemolysin; Molecular dynamics; Poisson–Nernst–Planck theory; Ion channel; Conductance

## 1. Introduction

The principal functional role in nature of ion channel proteins is to provide a conduction pathway for ions to cross a cellular lipid membrane. One such example of a membrane protein channel is the  $\alpha$ -hemolysin (33.2 kDa) produced by the *Staphylococcus aureus*  $\alpha$ -toxin. The polypeptide spontaneously self-assembles into a homo-heptameric channel and inserts itself into the cellular membrane. Leakage of ions and small organic molecules occurs leading to the lysis of the membrane and ultimately to the death of the cell [1]. A key property of the  $\alpha$ -hemolysin channel is that under physiological conditions it remains open for extended times. At a given voltage, the mean conductance of the  $\alpha$ -hemolysin channel varies linearly with the conductivity of the electrolyte solution [17,18]. The channel exhibits

a voltage-dependent instantaneous conduction, super-linear at positive voltages and sub-linear at negative voltages. Reverse potential experiments also show that the  $\alpha$ -hemolysin channel is slightly selective for anions. This selectivity is increased at lower pH.

Experimental studies with the  $\alpha$ -hemolysin protein inserted in a lipid bilayer show that, in 1.0 M KCl solution, a 120 mV applied potential produces a steady open channel ionic current of  $120 \pm 5$  pA [2,19]. Translocation of single-stranded nucleic acid polymers causes partial blockade of ionic current through the channel. The level of fractional blockade differs for various nucleic acid homopolymers making it possible to use nanopores for DNA sequencing [2–5]. However, the fast translocation rate ( $\sim 1$ –5 subunits per microsecond) and small differences in the levels of ionic current blockade present a challenge in signal-processing to achieve

\*Corresponding author. E-mail: vstolc@mail.arc.nasa.gov

<sup>¶</sup>Eloret Corporation, 690 W. Fremont Avenue, Suite 8, Sunnyvale, CA 94087-4202, USA.

the desired single nucleotide resolution [26]. To design a nanopore with such resolution and properly model the effect of polynucleotides translocation, the basic properties of ionic flux through the  $\alpha$ -hemolysin channel must first be simulated.

Present experimental techniques allow structural determinations with atomistic resolution [1]. This enables tracking of many aspects of the ion permeation process using molecular dynamics (MD) simulations. However, calculation of conductance based solely on this method is still beyond the current computational limit [6,8]. The time scale of physiological ion permeation is in the order of  $\sim 100\text{ ns} - 1\text{ }\mu\text{s}$  [15] while for a 100,000-atom system a reasonable upper limit with the present computer resources is about 10 ns [8]. To model events that occur at this time scale and to reduce the loss of information due to the averaging of some of the system's degrees of freedom, an appropriate strategy is to combine MD with continuum models such as Poisson–Nernst–Planck (PNP) or Eyring Rate Theory (ERT). Such a hierarchical approach allows a relatively quick computation of ionic fluxes and translocation times [6,8,9] once the critical information (structural details, transport coefficients, energies, etc.) has been extracted from MD [24,30].

This work combines MD with the PNP electrodiffusion theory to model ionic currents for the  $\alpha$ -hemolysin channel. The PNP model employs several simplifying assumptions. The solvent is approximated as a continuum in which polarized molecules are represented by a relative dielectric constant. The choice of the dielectric constants for both channel and solvent has a large impact on potential barriers resulting from fixed residues and polarization at the pore-channel boundary [43,44]. Typical values of  $\epsilon = 20$  in the protein and  $\epsilon = 80$  in the solvent have been successfully used to predict ion currents for protein channels like the bacterial porin OmpF [9,28] and gramicidin A [10]. Ions in PNP models are also represented as a continuum, where the ion concentration can be viewed as the un-normalized time-averaged probability of finding an ion at a point within the system. Ion current calculations using PNP theory require careful choice of ion diffusion coefficients and mobilities. In particular, the PNP theory may overestimate ion currents if cation–anion correlations and concentration dependent diffusion coefficients, especially at high concentrations, are not included [28]. The regime in which the use of the PNP theory may be critical is for channels such as gramicidin in which large fluctuations measured for ion currents suggest single-file motion of the ions. Despite this, the PNP approach has been found to accurately predict ion currents measured for channels with diameters as small as  $4\text{ }\text{\AA}$  [10,45]. In addition, the ion density inside a protein channel calculated from PNP calculations is consistent with MD calculations [28]. Thus, as long as the ratio of solvent molecules to ions does not become discontinuous, the use of average diffusion coefficients and relative dielectric constants to mediate interactions between charges seems valid.

The critical parameter to be determined from MD simulations is the diffusion coefficient of the ions within the pore. Besides the interaction with the water molecules, the diffusive motion of the ions is heavily influenced by the energy gradients produced by the channel protein. However, even if ion crossing events are not observed during the MD simulation time, an averaged diffusivity may still be used if the electrostatic potential of the protein is included in the PNP simulations. For various models of ion channels, the diffusion coefficient of ionic species was determined from the time evolution of the mean square displacement [15,25] or from the decay of the velocity autocorrelation function [24]. Ionic diffusivities were appreciably reduced by narrow channels and associated with a diminished exchange of water molecules (hydration). This decrease seems to be independent of the secondary structure of the channel. The presence of a strong dipole field may, however, induce a directional drift.

The goal of the present study is to combine atomistic MD and PNP simulations into a hybrid model in which all the parameters in the calculations are derived from structural data. This model is applied to predict the  $\alpha$ -hemolysin conductance properties by implementing structural details and ionic diffusion coefficients from MD simulations into PNP. Only dynamics of the ions that contribute to current flow is considered, while the position of the atoms that form the pore and their charges remain fixed. The PNP model calculates ionic fluxes by combining the solutions of both electro-diffusion and Poisson (electrostatic potential maps) equations. This hybrid model provides a more realistic description than pure Nernst–Planck models or PNP models that do not account for atomistic details.

## 2. Model of the $\alpha$ -hemolysin protein channel

The X-ray diffraction structure of the  $\alpha$ -hemolysin protein (figure 1), determined with a resolution of  $1.9\text{ }\text{\AA}$  at a temperature of  $287\text{ K}$  and under physiological conditions is available for downloading (code 7AHL) from the Protein Data Bank [1,20]. The protein has a symmetrical structure (space group C121) that contains a total of 2051 amino acid residues organized in seven sequence-identical chains denoted A–G (figure 1). The sequence of one of the chains is indicated in figure 2. The pore of the mushroom-shaped heptamer is  $\sim 100\text{ }\text{\AA}$  long and ranges in diameter from  $\sim 12\text{ }\text{\AA}$  in the transmembrane (stem) region to  $\sim 42\text{ }\text{\AA}$  in the extra cellular (cap) region [21,42]. The transmembrane domain is formed by a 14-strand antiparallel beta barrel and has a hydrophobic character towards the exterior while being primarily hydrophilic towards the inside.

For a more accurate determination of the pore internal diameters, the structure was first aligned with the pore axis along the  $z$  direction of the coordinate system, with the origin at the geometric center of the protein. The symmetry of the pore was then used to calculate the geometric center

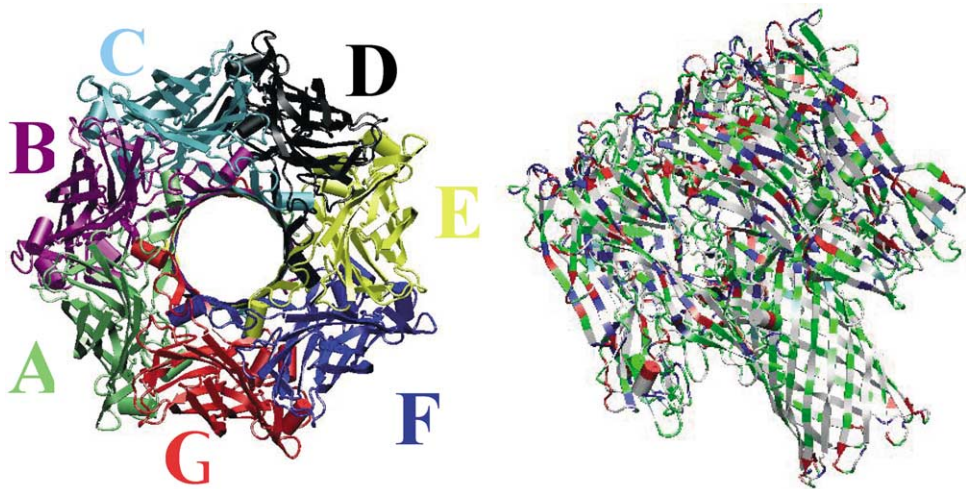


Figure 1. Cartoon representation of the  $\alpha$ -hemolysin protein. The frontal view on the left shows the seven individually colored chains (labeled A–G) that form the protein. For the lateral view on the right the amino acids are colored according to their charge and polar character: acidic in red, basic in blue, hydrophobic in white and hydrophilic in green.

for equivalent atom locations along the seven chains [42]. The diameter is the minimum average distance to the geometric center of the atom sets selected at each axial position (figure 3). According to these calculations, the pore mouth has a diameter of 30 Å that within the first 10 Å from the pore entrance narrows down to 20 Å. The length of this cap constriction is about 10 Å. The cap then widens again such that the region around the geometric center of the channel exhibits the largest cavity (diameter 42 Å) of the whole structure. The narrowest constriction of the pore ( $C_1$ ) is located another 10 Å down the axis channel, at the cap stem junction (figure 5).  $C_1$  is formed by two sets of amino acid pairs separated by approximately

6 Å: GLU (1 1 1) with LYS (1 4 7) and MET (1 1 3) with THR (1 4 5). The second pore constriction  $C_2$  is located closer to the pore-stem end (figure 5) and consists of a set of hydrophobic LEU (1 3 5) amino acids. This information is summarized in table 1.

The inner volume of the pore was calculated as the sum of the volume of cylinders 1 Å high with the diameter equal to the diameter of the pore corresponding to the axial position in the channel as shown in figure 3. A value of  $\sim 56,000 \text{ \AA}^3$  was calculated. A second value of  $\sim 48,000 \text{ \AA}^3$  was determined by calculating the Connolly volume [22] of the solvent molecules situated within the channel boundaries (figure 4) using a probe radius of

1 ALA	2 ASP	3 SER	4 ASP	5 ILE	6 ASN	7 ILE	8 LYS	9 THR	10 GLY
11 THR	12 THR	13 ASP	14 ILE	15 GLY	16 SER	17 ASN	18 THR	19 THR	20 VAL
21 LYS	22 THR	23 GLY	24 ASP	25 LEU	26 VAL	27 THR	28 TYR	29 ASP	30 LYS
31 GLU	32 ASN	33 GLY	34 MET	35 HID	36 LYS	37 LYS	38 VAL	39 PHE	40 TYR
41 SER	42 PHE	43 ILE	44 ASP	45 ASP	46 LYS	47 ASN	48 HID	49 ASN	50 LYS
51 LYS	52 LEU	53 LEU	54 VAL	55 ILE	56 ARG	57 THR	58 LYS	59 GLY	60 THR
61 ILE	62 ALA	63 GLY	64 GLN	65 TYR	66 ARG	67 VAL	68 TYR	69 SER	70 GLU
71 GLU	72 GLY	73 ALA	74 ASN	75 LYS	76 SER	77 GLY	78 LEU	79 ALA	80 TRP
81 PRO	82 SER	83 ALA	84 PHE	85 LYS	86 VAL	87 GLN	88 LEU	89 GLN	90 LEU
91 PRO	92 ASP	93 ASN	94 GLU	95 VAL	96 ALA	97 GLN	98 ILE	99 SER	100 ASP
101 TYR	102 TYR	103 PRO	104 ARG	105 ASN	106 SER	107 ILE	108 ASP	109 THR	110 LYS
111 GLU	112 TYR	113 MET	114 SER	115 THR	116 LEU	117 THR	118 TYR	119 GLY	120 PHE
121 ASN	122 GLY	123 ASN	124 VAL	125 THR	126 GLY	127 ASP	128 ASP	129 THR	130 GLY
131 LYS	132 ILE	133 GLY	134 GLY	135 LEU	136 ILE	137 GLY	138 ALA	139 ASN	140 VAL
141 SER	142 ILE	143 GLY	144 HID	145 THR	146 LEU	147 LYS	148 TYR	149 VAL	150 GLN
151 PRO	152 ASP	153 PHE	154 LYS	155 THR	156 ILE	157 LEU	158 GLU	159 SER	160 PRO
161 THR	162 ASP	163 LYS	164 LYS	165 VAL	166 GLY	167 TRP	168 LYS	169 VAL	170 ILE
171 PHE	172 ASN	173 ASN	174 MET	175 VAL	176 ASN	177 GLN	178 ASN	179 TRP	180 GLY
181 PRO	182 TYR	183 ASP	184 ARG	185 ASP	186 SER	187 TRP	188 ASN	189 PRO	190 VAL
191 TYR	192 GLY	193 ASN	194 GLN	195 LEU	196 PHE	197 MET	198 LYS	199 THR	200 ARG
201 ASN	202 GLY	203 SER	204 MET	205 LYS	206 ALA	207 ALA	208 ASP	209 ASN	210 PHE
211 LEU	212 ASP	213 PRO	214 ASN	215 LYS	216 ALA	217 SER	218 SER	219 LEU	220 LEU
221 SER	222 SER	223 GLY	224 PHE	225 SER	226 PRO	227 ASP	228 PHE	229 ALA	230 THR
231 VAL	232 ILE	233 THR	234 MET	235 ASP	236 ARG	237 LYS	238 ALA	239 SER	240 LYS
241 GLN	242 GLN	243 THR	244 ASN	245 ILE	246 ASP	247 VAL	248 ILE	249 TYR	250 GLU
251 ARG	252 VAL	253 ARG	254 ASP	255 ASP	256 TYR	257 GLN	258 LEU	259 HID	260 TRP
261 THR	262 SER	263 THR	264 ASN	265 TRP	266 LYS	267 GLY	268 THR	269 ASN	270 THR
271 LYS	272 ASP	273 LYS	274 TRP	275 THR	276 ASP	277 ARG	278 SER	279 SER	280 GLU
281 ARG	282 TYR	283 LYS	284 ILE	285 ASP	286 TRP	287 GLU	288 LYS	289 GLU	290 GLU
291 MET	292 THR	293 ASN							

Figure 2. The amino acids sequence of one of the seven chains (A–G) that form the  $\alpha$ -hemolysin protein channel. The total charge per protein chain is  $+1e^-$  as the sum of positively (ASP, red; GLU, pink) and negatively (LYS, blue; ARG, green) charged amino acids. The yellow highlighted amino acids were selected for the reduced model of the pore in the MD simulations. For the pore stem used in the PNP model, the pink highlighted sequence was considered.

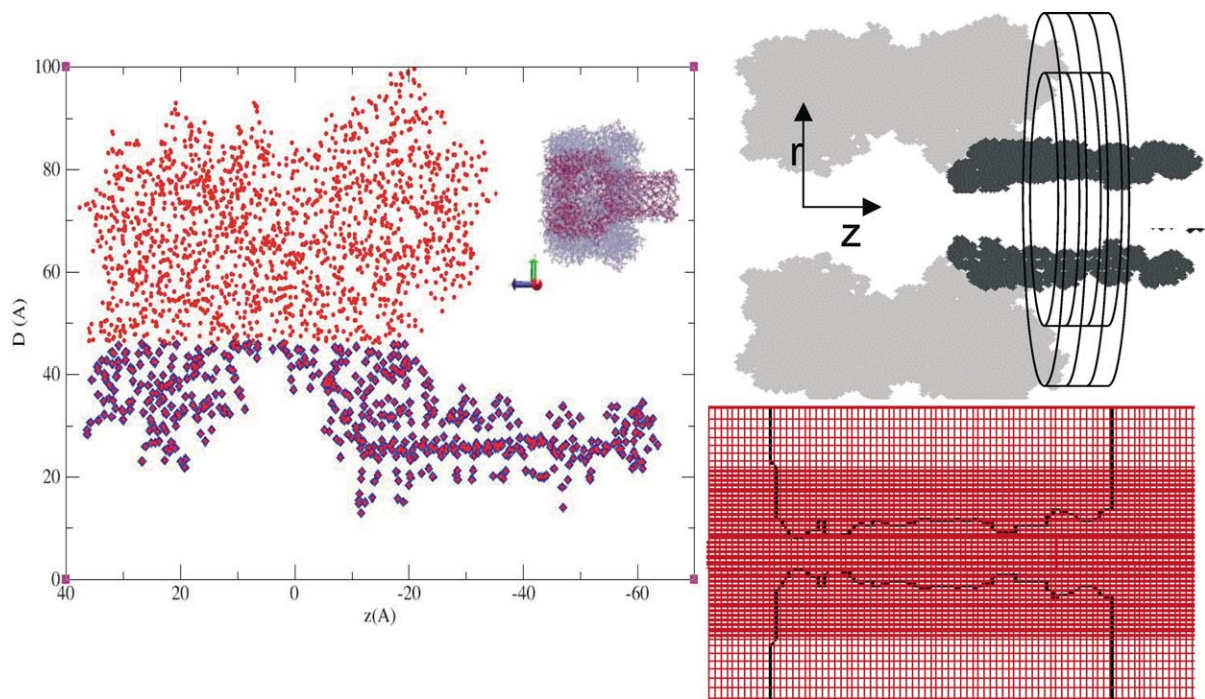


Figure 3. Left: Projection in the axial plane of the  $\alpha$ -hemolysin channel. The internal diameter of the pore corresponding to each position  $z$  along the channel axis is shown. The blue points represent the selection for the “reduced” representation of the pore used in the MD calculations of ion diffusion coefficients. The inset shows the reduced representation (purple) overlapped on the full  $\alpha$ -hemolysin structure (blue). Right: Schematic representation of  $\alpha$ -hemolysin channel. In the PNP model a 2D grid (represented as concentric rings) corresponding to a cylindrical polar coordinate system is applied over the pore stem (dark area).

1.5 Å. Thus, when solvated in a 1 M KCl solution, the pore should contain about  $\sim 30$ – $34$  ion pairs and about  $\sim 1665$  water molecules (in a 1 M solution there are approximately 55 water molecules per ion pair).

The following residues had missing atoms in the X-ray structure and were replaced from the amino acid library of InsightII (Accelrys Inc.) molecular graphics software package: ARG66 and LYS75 in chain A, LYS30 and LYS240 in chain D, LYS283 and LYS30 in chain F. To reproduce conditions in the polymer translocation experiments [2–4],  $\alpha$ -hemolysin (32,305 atoms) was protonated at neutral pH, resulting in a positively ( $+7e^-$ ) charged structure. The amino and carboxyl termini were patched with  $NH_3^+$  and  $COO^-$  groups, respectively.  $Cl^-$

counter ions were added to neutralize the system using the Amber7 software [13]. The Cornell 95 [12] force field was used to assign parameters for the potential functions and partial charges on the atoms. To minimize the energy of the structure, 250 steps of steepest descent followed by 1250 steps of conjugated gradient method were used in Amber7. By repeating this procedure, hydrogen atoms were minimized first, followed by side chains, all atoms except the  $\alpha$ -carbons and finally all atoms. The RMSD value calculated for all the atoms was 0.8 Å, indicating that no significant deviation occurred during minimization.

In the MD simulations, a simplified atomistic representation of the protein was generated in which all the residues of those  $\alpha$ -carbons positioned within 25 Å of the channel axis were selected (figure 3). The reduced representation of the pore had a total charge of  $14e^-$  and was neutralized by adding  $K^+$  counter ions. The atoms forming the pore were not allowed to move during any of the simulations presented in this study.

From each of the seven protein chains, an overall neutral sequence (LYS110–LYS147) was also selected (figure 2) as a model for the pore stem in the PNP calculations. Although this selection has a zero total net charge, it corresponds to a total dipole of  $\sim 1500$  D. The dipole positive charge center is located at the cap-stem junction, and it originates from the larger number of positively charged LYS (14) amino acids over the negatively charged GLU (only 7) amino acids. The dipole negative charge center is located at the stem end where there are more

Table 1. The  $\alpha$ -hemolysin pore stem constrictions.

Constriction	Amino acid	Pore radius (Å)	Type	Axial position (Å)
C <sub>1</sub>	GLU (111)	7.4	Acid	−11.9
	LYS (147)	6.1	Basic	−14.2
	MET (113)	6.4	Hydrophobic (non-polar)	−18.3
	THR (145)	8.2	Hydrophilic (polar)	−20.4
C <sub>2</sub>	LEU (135)	6.3	Hydrophobic (non-polar)	−47.3

The axial position of the amino acids forming the two constrictions is measured from the pore geometric center (set at the origin of the system of coordinates).

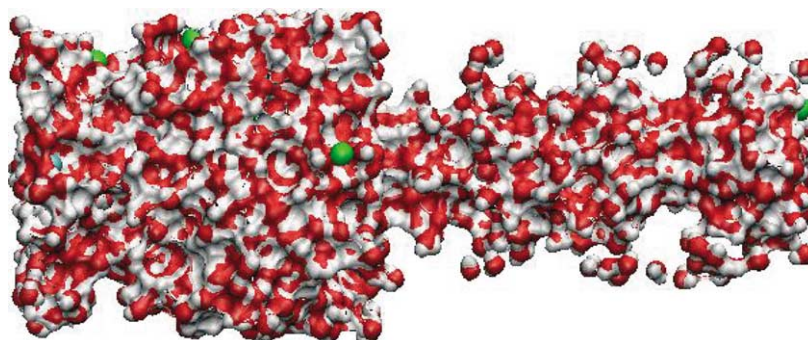


Figure 4. Connolly surface of the solvent selection inside the  $\alpha$ -hemolysin channel. The Cerius2 software [Accelrys Inc.] was used to generate the image.

negatively charged ASP (14) amino acids than LYS (7) amino acids. The two centers are separated by a distance of  $\sim 47$  Å (figure 5). The pore stem atoms of this selection are included within a continuum boundary defined in the PNP calculations (“Poisson–Nernst–Planck calculations” section).

### 3. MD calculations

MD simulations were conducted using the NAMD software [11] on NASA-Ames Research Center (SGI, Origin 3000) supercomputers. A switching function

was used to calculate the non-bonded interactions with a switch distance of 17.5 Å and a cutoff of 18.5 Å. To speed up the calculations and obtain longer MD timescales, a multiple time step algorithm (MTS) was used where the non-bonded interactions are evaluated periodically [40]. NAMD uses a non-bonded pair list that includes all pairs of atoms within a certain distance that may be updated periodically. The pair list distance was set in the present calculations to 20 Å and updated every 20 MD integration steps. Within the 20 steps cycle, the van der Waals and electrostatic interactions were updated at intervals of 2 and 4 steps, respectively. Also, to speed up the calculations, the RATTLE algorithm [16] was used to

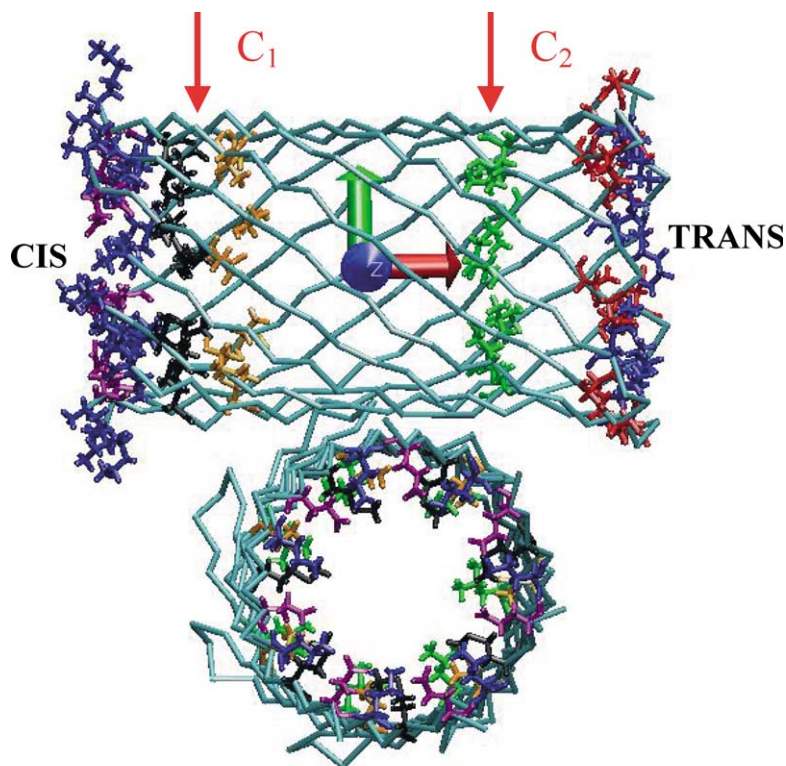


Figure 5. Top: Lateral view of the pore stem. The location of the charged amino acids is shown using the following color code: LYS in blue, ASP in red, GLU in pink. The location of the two constrictions ( $C_1$  and  $C_2$ ) is indicated by the red arrows.  $C_1$  is formed by GLU, LYS, MET (orange) and THR (black).  $C_2$  is formed by a set of LEU (green) residues. Bottom: View perpendicular to the channel axis. Only the amino acids that form the two constrictions are shown.

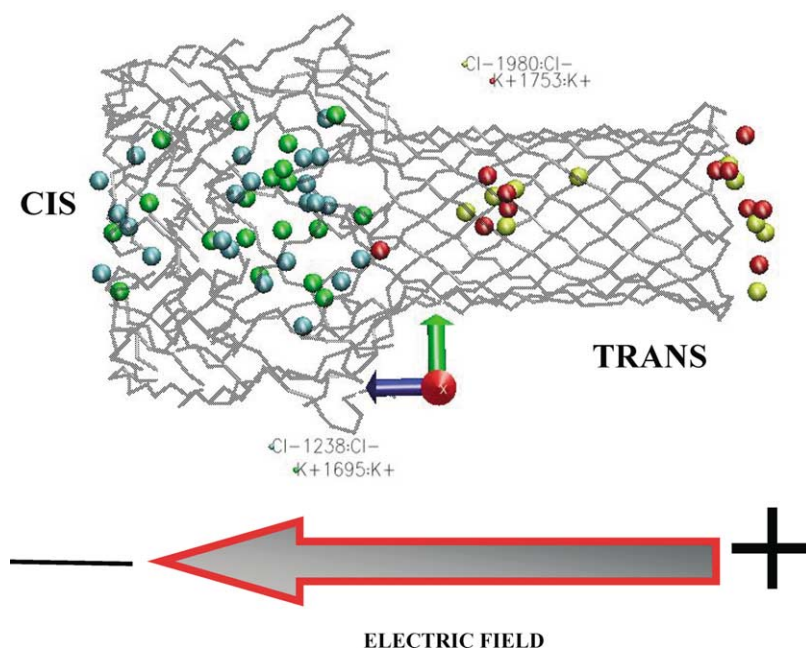


Figure 6. Snapshot from an MD simulation of the  $\alpha$ -hemolysin system in a 1 M KCl solution and an external applied electric field. The following selections for the ions are shown as van der Waals spheres:  $K^+$  ions inside the pore cap (light green),  $Cl^-$  ions inside the pore cap (light blue),  $K^+$  ions inside the pore stem (yellow) and  $Cl^-$  ions inside the pore stem (red). The solvent molecules (SPC/E water) are not displayed.

constrain all the bonds involving hydrogen atoms, thus allowing an increase in MD integration time to 2 fs. The Particle Mesh Ewald method [41] was used to evaluate the long-range electrostatics.

The following equilibration procedure was used for MD simulations:

1. 5000 iteration steps of energy minimization.
2. 35,000 time steps during which the system was heated from 50 to 300 K at every 5000 steps using the method of velocity reassignment.
3. 350,000 time steps of MD equilibration (equivalent to 700 ps) at 300 K using the MTS-NPT ensemble and the Berendsen thermostat and barostat.
4. 500,000 time steps of MD production (equivalent to 1 ns) at 300 K using the NVE ensemble and an external applied electric field. An electric field of  $0.029 \text{ kcal/mol/\AA/e}^-$  (equivalent to the experimental value of 125 mV over the 100 Å long pore) is uniformly applied along the channel axis (figure 6).

The electrolyte solution consisted of a combination of SPC/E water molecules,  $K^+$  ions and  $Cl^-$  ions. The extended simple point charge (SPC/E) model [23] was selected because it describes more accurately the dynamical (diffusion) and structural properties of liquid water at room temperature compared to other models [23,32] and seems to be more appropriate to model properties of ionic solutions [27]. The intermolecular potential of SPC/E uses a Lennard–Jones (12–6) interaction between the oxygen atoms and Coulomb interactions between partial electronic charges on the H ( $q(H) = 0.4238e^-$ ) and O ( $q(O) = -0.8476e^-$ ) atoms.

The SHAKE algorithm [34] is required by this model to conserve intramolecular constraints ( $r(OH) = 1 \text{ Å}$ ,  $\theta(HOH) = 109.47^\circ$ ).

Roux parameters optimized from free energy calculations are used for both cations ( $K^+$ ) and anions ( $Cl^-$ ) [31]. The solvation energy for  $K^+$  is  $-79.6 \text{ kcal/mol}$  and for  $Cl^-$  is  $-79.4 \text{ kcal/mol}$ . The van der Waals parameters for both the water model and for the ions are summarized in table 2. For the off diagonal terms, the Lorentz–Berthelot mixing rules were used: geometric for the energy parameters ( $\epsilon$ ) and additive for the radii parameters ( $R^*$ ) [12].

The properties of the water model were verified for a box of SPC/E water molecules (2790 residues, cubical UC,  $L \sim 48 \text{ Å}$ ) at 300 K. The first peak of the radial distribution of oxygen–oxygen atoms is located at 3 Å and has a height of  $g_{OO} = 2.5$ , and the diffusion coefficient of the water molecules in the SPC/E model was calculated to be  $2.7 \times 10^{-9} \text{ m}^2/\text{s}$ . The density and average potential energy calculated in our simulations are  $0.998 \text{ g/cc}$  and  $-9.89 \text{ kcal/mol}$  of molecule, respectively. This structural information is consistent with experimental [33] and modeling evidence [23,32].

To generate a periodic structure of the 1 M KCl solution, the atom arrangement of the NaCl crystal in

Table 2. Electrolyte solution Lennard–Jones parameters [23,31].

	$\sigma$ (Å)	$\epsilon$ (kcal/mol)
O–O*	1.7767	0.1553
$K^+$ – $K^+$	1.76375	–0.087
$Cl^-$ – $Cl^-$	2.27	–0.15

which the  $\text{Na}^+$  atoms were replaced by  $\text{K}^+$  atoms, was considered. The original unit cell (UC) is cubical ( $\sim 5.6 \text{ \AA}$ ) and contains 4 KCl pairs. First, a super cell was constructed using the Cerius2 molecular software (Accelrys Inc.) by considering two copies of the original UC in each of the three space directions and removing one pair of ions. This super cell was solvated and then equilibrated at room temperature. The dimensions of the equilibrated box are approximately  $30 \times 30 \times 45 \text{ \AA}^3$ . A super cell of dimensions  $90 \times 90 \times 135 \text{ \AA}^3$  was then generated by repeating three times the original cell in each direction of space. This final model contained 621 KCl pairs and 40,959 water molecules (approximate ratio of 66). This structure was energy minimized over 1000 steps, heated from 50 up to 300 K in steps of 50 K every 10 ps, and equilibrated for 200 ps at 300 K using the NPT ensemble with the Berendsen temperature and pressure coupling [34]. The diffusion coefficients of the two ion species are determined to be:  $1.8 \times 10^{-9} \text{ m}^2/\text{s}$  for  $\text{K}^+$  and  $1.5 \times 10^{-9} \text{ m}^2/\text{s}$  for  $\text{Cl}^-$ . Reference values are  $1.83 \pm 0.05 \times 10^{-9} \text{ m}^2/\text{s}$  for  $\text{K}^+$  and  $1.8\text{--}2.9 \times 10^{-9} \text{ m}^2/\text{s}$  for  $\text{Cl}^-$  [36–38].

This pre-equilibrated UC containing KCl solution was then superimposed over the  $\alpha$ -hemolysin structure. Overlapping ions and water molecules were removed and added back randomly to the UC to preserve the 1M concentration. The pore was fixed, and the procedure described in the beginning of the third section was followed.

If the entire  $\alpha$  hemolysin structure is solvated into a periodic cell of approximately  $\sim 130 \text{ \AA}$ , the system contains 175,364 atoms. Using a cutoff value of  $20 \text{ \AA}$  to calculate the long-range terms in the energy expression and a 2 fs integration time of the equations of motion, 3.52 days on 128 processors are required to reach 1 ns of MD when fixed constraints are applied on the protein. Comparatively, the reduced system consists of only  $\sim 120,000$  atoms when fully solvated and reaches 1 ns MD time on 200 processors in 1.3 days run-time again if the protein geometry is held fixed. For reasons of computational efficiency, in the present MD simulations the “reduced” representation of the protein (figure 3) was used.

Figures 1, 5 and 6 were generated with the visual molecular dynamics (VMD) software developed by the Theoretical and Computational Biophysics Group in the Beckman Institute for Advanced Science and Technology at the University of Illinois at Urbana-Champaign [14].

#### 4. Poisson–Nernst–Planck calculations

Based on a simple scaling of the resistance with the pore cross-sectional area, most of the external potential difference applied experimentally over the pore drops linearly across the pore stem. To solve the 2D PNP equations, the pore stem was idealized by a smooth cylinder of radius  $8.75 \text{ \AA}$  to which the two constrictions ( $C_1$  and  $C_2$ )

were added as solid blocks of widths 11 and  $3 \text{ \AA}$ , respectively. As such, at these locations, the radius is reduced to  $6.75 \text{ \AA}$ . The atomistic charges are included within the cylinder boundaries. A discretized grid of concentric rings with a resolution of  $0.5 \text{ \AA}$  that corresponds to a cylindrical polar coordinate system was then considered (figure 3). In the axial direction, the pore occupies approximately 60% of the total grid space. The values of the dielectric constant of the pore and of the ionic solution are 20 and 80, respectively [30]. All PNP calculations in the present study were performed for a 1 M KCl solution.

In contrast to the MD calculations where discrete ion positions are considered, the PNP approach assumes a continuum distribution of ions. The ion concentration at a location is calculated as the time-averaged un-normalized probability of finding an ion at that location.

In one of the earliest forms, a reduced one-dimensional PNP implementation was used to describe ion permeation [47]. Extension of the theory to realistic 3-D cases has only recently been achieved [48]. Following the formalism of Hollerbach *et al.* [10], in the present approach a 2D-Poisson equation is used that relates the electrostatic potential  $\phi$  to the fixed charge density  $\rho_F$  and to the concentrations of the positive  $C_p$  and negative  $C_n$  carriers.

$$\nabla \epsilon_r \nabla \phi = -\frac{q}{\epsilon_0}(C_p - C_n + \rho_F) \quad (1)$$

where  $\epsilon_r$  and  $\epsilon_0$  are the relative and vacuum permittivities and  $q$  is the charge of the ionic carriers. The two concentrations are set initially at the bulk ion concentration.

The total potential is calculated as the sum of the potential contribution from fixed atomic charges  $\Phi_F$  and of the potential contribution due to the ions,  $\Phi_D$ :

$$\phi = \Phi_F + \Phi_D \quad (2)$$

As the value of the atomic charges is fixed during the simulation,  $\Phi_F$  is evaluated only once from the following Poisson equation:

$$\nabla \epsilon_r \nabla \Phi_F = -\frac{q}{\epsilon_0}(\rho_F) \quad (3)$$

Effects of surface polarization at the dielectric boundary and the external applied potential are also included in equation (3). The contribution from the ionic species,  $\Phi_D$ , is variable, and it is calculated iteratively:

$$\nabla \epsilon_r \nabla \Phi_D = -\frac{q}{\epsilon_0}(C_p - C_n). \quad (4)$$

Next, the ion flux,  $J$ , for each ion species ( $p$  for positive carriers and  $n$  for negative carriers) is approximated by the Nernst–Planck drift–diffusion equation:

$$J_i = q\mu_i C_i [-\nabla \phi] - qD_i \nabla C_i, \quad i \in \{p, n\} \quad (5)$$

$$\nabla \cdot J_i = 0 \quad (6)$$

$$\mu_i = D_i \frac{q}{k_B T} \quad (7)$$

where  $D_i(\text{m}^2/\text{s})$  is the ion species diffusion coefficient,  $\mu_i(\text{m}^2/\text{Vs})$  the corresponding mobility calculated from equation (7),  $k_B (J/K)$  is the Boltzmann constant,  $T (K)$  is the absolute temperature and  $e (C)$  is the charge of an electron. Equation (5) relates the current for each ion species to the force on the ion (first term) and the concentration gradients of the ion species (second term). The conservation condition given by equation (6) simply states that the ionic current must be conserved at steady state. Equations 1–7 are solved iteratively for the potential profile  $\phi$  and the equilibrium ion concentrations  $C_i$ . The ionic current  $I$  is calculated by integrating the flux of positive and negative ions over the channel cross section (dA):

$$I = \int (J_n + J_p) dA \quad (8)$$

The equations are solved using a finite difference technique implemented in the SEMS code, which was previously used to model plasma flow [35]. The convergence of the solution is ensured by the fact that within 400 simulation steps (the average iteration steps of a PNP run in this study) the residuals have decreased about 4 orders of magnitude.

Although for narrow channels PNP tends to overestimate conductance properties [28], it has been used with considerable success to calculate average ion fluxes in a variety of biological systems [9,10,45].

## 5. Results and discussion

### 5.1 Diffusion coefficients

Einstein showed for three-dimensional systems that, for long times, the mean square displacement of the diffusing particle is proportional to the time, following:

$$6D_t = \langle |r_i(t) - r_i(0)|^2 \rangle \quad \text{as } t \rightarrow \infty \quad (9)$$

where  $r_i(t)$  is the position vector of the particle at time  $t$ ,  $D$  is the diffusion coefficient and  $\langle \rangle$  means average over particles [46]. MD simulations allow us to calculate the mean square displacement, MSD (right hand side term in equation (9)) as a function of time. This equation is most accurate when applied for situations in which the system has reached the diffusive regime (linear relationship between the mean square displacement and time). For ions in concentrated solutions, to compute transport coefficients one has to significantly exceed the characteristic Debye time, usually requiring time scales of nanoseconds [6,8,36–38]. For example, for simple 1–1 electrolyte solutions in the molar range the value of the Debye time is about 100 ps.

For the purpose of the present study, the diffusion coefficients are calculated for the following five selections including all ions for each ionic species

( $K^+$  and  $Cl^-$ ) within:

1. the UC (622  $Cl^-$  and 636  $K^+$ )
2. the UC but not the  $\alpha$ -hemolysin pore (592  $Cl^-$  and 610  $K^+$ )
3. the  $\alpha$ -hemolysin pore (30  $Cl^-$  and 26  $K^+$ )
4. the  $\alpha$ -hemolysin cap (23  $Cl^-$  and 20  $K^+$ )
5. the  $\alpha$ -hemolysin stem (7  $Cl^-$  and 6  $K^+$ )

Selections 3–5 are shown in figure 6 in which the ions are represented as differently colored van der Waals spheres for the cap and stem sections of the pore. Only the few ions from the bulk solution located in the close proximity of the pore that enter the pore early during the dynamics are included in these selections.

The reason why there are more cations than anions in the UC is that 14 of the  $K^+$  ions are used to neutralize the pore. These ions were not held fixed during the simulation time and were considered in the diffusion coefficient calculations for selections 1 and 2.

The time evolution of the MSD for these five selections for the  $K^+$  and  $Cl^-$  ions from the 1 ns MD production runs is shown in figure 7. The diffusion coefficients are then calculated using equation (9), and the values are summarized in table 3. The values of the standard deviations in table 3 are calculated from six repeated MD runs using different random initial seeds to initialize the atomic velocities. Of the six MD runs, the initial run is 1 ns long and the five additional runs are 500 ps long. The percent error in table 3 indicates the percentage from the mean value represented by the standard deviation.

The bulk  $K^+$  ions have a slightly larger diffusion coefficient than the  $Cl^-$  ions. This difference is expected, based on the smaller solvation energy of  $Cl^-$  ions compared to  $K^+$  ions (see values in “MD calculations” section). For comparison, a box with pure 1 M KCl ionic solution containing 621 ion pairs ( $94 \times 94 \times 140 \text{ \AA}^3$ ) has diffusion coefficients of  $1.8 \times 10^{-9} \text{ m}^2/\text{s}$  for  $K^+$  and  $1.5 \times 10^{-9} \text{ m}^2/\text{s}$  for  $Cl^-$ , determined from 550 ps of MTS-NVE dynamics. These values are smaller than those calculated for selections 1 and 2. The presence of the  $\alpha$ -hemolysin pore in the UC seems to lead to an increase in the overall motion of the ions in the bulk solution (selection 2), most probably due to electrostatic potential of the protein. By adding to selection 2 the ions within the pore boundaries (selection 3) that have a more restricted motion, the diffusion coefficient is slightly decreased (selection 1). For both ionic species, the diffusion coefficients inside the pore (selections 3–5) are five to seven times smaller than for the bulk ions. Mainly due to geometric constraints, ionic channels are known to have restrictive effects on the motion of ions [15,25]. Additionally, the average value of  $Cl^-$  diffusion coefficients inside the pore boundary is slightly larger than that of the  $K^+$  ions.

Within the pore, the cap has a larger cavity and is able to accommodate more ions ( $\sim 23$  pairs) than the stem ( $\sim 7$  pairs). The diffusion coefficients of the ions in the cap are also larger than those calculated for the stem selection

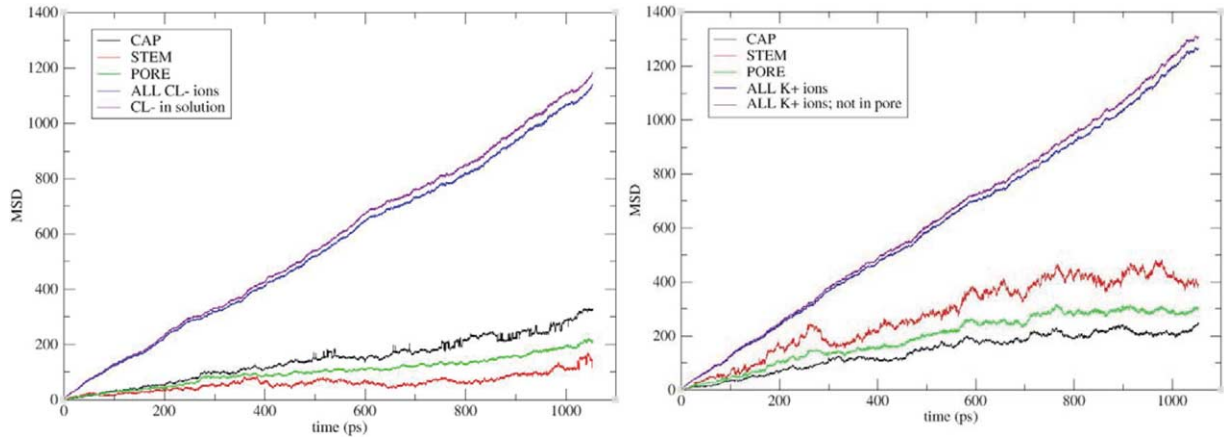


Figure 7. Mean square displacement versus time for  $\text{Cl}^-$  ions (left) and  $\text{K}^+$  ions (right) from 1 ns MD. The following selections are considered: all ions in the UC (blue line), all ions in the UC but not within the  $\alpha$ -hemolysin pore (purple line), ions inside the  $\alpha$ -hemolysin pore (green line), ions inside the  $\alpha$ -hemolysin cap (black line) and ions inside the  $\alpha$ -hemolysin stem (red line).

also having a lower precision because of reduced statistics. As the pore stem forms the narrower part of the channel, only a few ions are present at a time inside. This is reflected in the variation with time of the mean square displacement (figure 7): the lines are smooth for the large selections of ions in the bulk solutions but exhibit strong fluctuations for selections containing small number of ions (especially the red line in figure 7 that corresponds to the selection of ions within the pore stem). The percentages represented by the standard deviations from the mean values (table 3) calculated for the pore ions selections also exhibit larger values (17–46%) compared to the bulk ions selections ( $\sim 3\%$ ).

The presence of the ionic channel introduces inhomogeneities in the system, as the motion of the ions usually becomes preferential in one direction versus the others. Thus, it is meaningful to calculate separately the parallel ( $D_{\parallel}$ ) and perpendicular ( $D_{\perp}$ ) components of the diffusion coefficients.

With the channel oriented parallel to the space Oz axis, the two components of the ionic diffusivities

are by definition:

$$D_{\parallel} = \frac{\langle |z_i(t) - z_i(0)|^2 \rangle}{2t} \quad \text{as } t \rightarrow \infty \quad (10)$$

$$D_{\perp} = \frac{\langle |x_i(t) - x_i(0)|^2 \rangle + \langle |y_i(t) - y_i(0)|^2 \rangle}{4t} \quad (11)$$

as  $t \rightarrow \infty$ .

These components are evaluated for selections 3–5, and the values are summarized in table 4. Again, the standard deviations in table 4 are calculated from six repeated MD runs using different random initial seeds to initialize the atomic velocities. The correlation coefficients indicated between brackets in table 4 are a measure of the deviation of the time variation of the mean square displacement from the linear regime. As the value of the correlation coefficient approaches one, the fit is closer to linear.

Due to poor statistics, the total, axial and radial diffusion coefficients of the ions inside the pore stem are determined from linear fits characterized by low correlation coefficients and have large statistical uncertainties (40–60%). However, the data seem to point that for the ions located inside the pore stem the axial movement is dominant and is larger for  $\text{K}^+$  than for  $\text{Cl}^-$ . Inside the pore cap, the axial component still dominates over the radial component, but this time there seems to be a somewhat stronger drift of the  $\text{Cl}^-$  ions than of the  $\text{K}^+$  ions towards the protein walls. The radial components of the ionic diffusivities within the pore are determined by the interaction with the atoms on the pore walls and have comparable values with the axial diffusivities.

The diffusion coefficients in tables 3 and 4 are determined for a 120 mV applied external voltage ( $\Delta V$ ). In principle, by performing equilibrium MD simulations, the additional energy resulting from the external field should be dissipated. For small external voltages, far from

Table 3. Diffusion coefficients of the  $\text{K}^+$  and  $\text{Cl}^-$  ions for five different selections and for a 120 mV external applied voltage.

Ions selection	$D_{\text{K}^+}$ ( $10^{-9} \text{ m}^2/\text{s}$ )	% Error	$D_{\text{Cl}^-}$ ( $10^{-9} \text{ m}^2/\text{s}$ )	% Error
All within UC	$1.99 \pm 0.05$	2.5	$1.81 \pm 0.05$	2.8
All within UC not in the pore	$2.80 \pm 0.35$	12.5	$1.88 \pm 0.05$	2.7
Within the pore	$0.42 \pm 0.08$	19.1	$0.48 \pm 0.17$	35.4
Within the pore cap	$0.44 \pm 0.08$	18.2	$0.53 \pm 0.09$	16.9
Within the pore stem	$0.37 \pm 0.09$	24.3	$0.33 \pm 0.15$	45.5

The standard deviations are calculated from six repeated MD runs using different random initial seeds for atomic velocities initialization. The percent error indicates the percentage from the mean value represented by the standard deviation.

Table 4. Axial ( $D_{\parallel}$ ) and radial ( $D_{\perp}$ ) components of the diffusion coefficients for both ionic species inside the pore, pore cap and pore stem.

Selection	Ion	D ( $10^{-9}$ m <sup>2</sup> /s)	$D_{\parallel}$ ( $10^{-9}$ m <sup>2</sup> /s)	$D_{\perp}$ ( $10^{-9}$ m <sup>2</sup> /s)
Inside the pore	26 K <sup>+</sup>	0.42 ± 0.08 (0.89)	0.53 ± 0.16 (0.95)	0.37 ± 0.08 (0.93)
	30 Cl <sup>−</sup>	0.48 ± 0.17 (0.93)	0.58 ± 0.18 (0.98)	0.43 ± 0.09 (0.95)
Inside the pore cap	20 K <sup>+</sup>	0.44 ± 0.08 (0.91)	0.53 ± 0.14 (0.95)	0.39 ± 0.09 (0.93)
	23 Cl <sup>−</sup>	0.53 ± 0.09 (0.97)	0.67 ± 0.15 (0.85)	0.47 ± 0.08 (0.96)
Inside the pore stem	6 K <sup>+</sup>	0.37 ± 0.09 (0.86)	0.47 ± 0.18 (0.5)	0.32 ± 0.11 (0.52)
	7 Cl <sup>−</sup>	0.33 ± 0.15 (0.78)	0.41 ± 0.16 (0.73)	0.30 ± 0.16 (0.76)

The values of the correlation coefficients corresponding to a least square fit are indicated between brackets.

the plasma regime, the diffusion coefficient of ions should be independent of the value of the external electric field. To calculate the current voltage characteristics for the  $\alpha$ -hemolysin channel, based on the fluctuation–dissipation argument, one could use the diffusion coefficient determined for 120 mV. Thus, it is more of an academic exercise to study the dependence of the diffusion coefficients of both K<sup>+</sup> and Cl<sup>−</sup> ions as a function of  $\Delta V$ . One-nanosecond long MD simulations were repeated for a range of  $\Delta V$  between 30 and 240 mV. The diffusion coefficients for selections 2 and 3 as defined in the beginning of this section are calculated according to Eq. (9) and are summarized in table 5.

Indeed, for both K<sup>+</sup> and Cl<sup>−</sup> ions in the bulk solution and within the pore boundary, the variation in the calculated diffusion coefficients is less than 15%. This variation falls within the error range with which the diffusion coefficients are determined (table 3), suggesting that for small voltages, the diffusion coefficients are independent of  $\Delta V$ .

The diffusion coefficients determined for the whole pore are calculated from a better fit than for the pore cap or stem and represent best the “average” effect of the protein on the ions. In addition, as there seems to be no noticeable effect of the external applied voltage on the diffusion coefficients, the values determined at 120 mV are further used in the PNP model to study the conductance properties of the  $\alpha$ -hemolysin channel.

### Ionic currents

The total ionic current with its anionic and cationic components are calculated via the PNP model over a range of external applied voltages varying from −240 to

240 mV. Experimental data is available for a 0.1 M KCl solution for a smaller voltage range (−150–150 mV) [17]. To compare the present calculations with the experimental determinations, the experimental data were rescaled under the following assumptions. The KCl solution is known to be a strong electrolyte [29,39]. A linear relationship thus exists between the  $\alpha$ -hemolysin conductance and the solution molarity. In addition, experimental evidence [17] indicates that for a constant voltage a linear relationship also exists between the mean conductance of the  $\alpha$ -hemolysin channel and the conductivity of the electrolyte solution for different KCl concentrations. Thus, the values of the ionic current measured at 0.1 M should be scaled up by a factor of 10 (the ratio between molarities) to generate the I–V characteristic corresponding to a 1 M concentration. A second order polynomial was fit using the least square procedure through the rescaled experimental data points (residual  $R^2 = 0.99$ ). These fitted parameters were then used to generate the experimental values of the ionic current at a molarity of 1 M for voltage values between −150 and 150 mV.

Both experiments (triangles in figure 8) and simulations (squares in figure 8) show that the  $\alpha$ -hemolysin channel has a rectifying behavior: superlinear at positive applied  $\Delta V$  and sublinear for negative values of  $\Delta V$ . For reference, the I–V characteristic of a smooth cylinder of constant radius was also calculated (diamonds in figure 8) showing that in the absence of charges and geometrical variations, a linear dependence exists.

A value of 120 pA for the open channel ionic current is referenced in the translocation experiments performed with the  $\alpha$ -hemolysin channel [2–4,19]. This value is determined for an applied 120 mV voltage and for a 1 M KCl solution. Other studies [17,18] also reference the conductance of the  $\alpha$ -hemolysin channel as being  $\sim 1$  ns corresponding to an applied 120 mV voltage.

Considering the pore ions diffusion coefficients and the associated uncertainties calculated from six repeated MD runs (table 3), the ionic current corresponding to a 120 mV voltage drop is  $150.9 \pm 31.5$  pA of which  $\sim 60\%$  originates from the anions and  $\sim 40\%$  from the cations. The pore conductance is  $1.26 \pm 0.26$  ns. Within the determined standard deviations, the calculated values for the open channel ionic current and conductance are in good agreement with the existing experimental evidence (figure 8). The dominating contribution from the anions

Table 5. Diffusion coefficients of the K<sup>+</sup> and Cl<sup>−</sup> ions for a range of external applied potentials  $\Delta V$  between 30 and 240 mV

$\Delta V$ (mV)	$D_{K^+}$ ( $10^{-9}$ m <sup>2</sup> /s)		$D_{Cl^-}$ ( $10^{-9}$ m <sup>2</sup> /s)	
	Solution	Pore	Solution	Pore
30	1.89	0.41	1.71	0.49
60	2.12	0.38	1.79	0.49
90	1.96	0.42	1.85	0.48
120	2.01	0.38	1.81	0.31
150	2.14	0.42	1.8	0.36
210	2.3	0.45	1.89	0.46
240	2.2	0.44	1.84	0.55

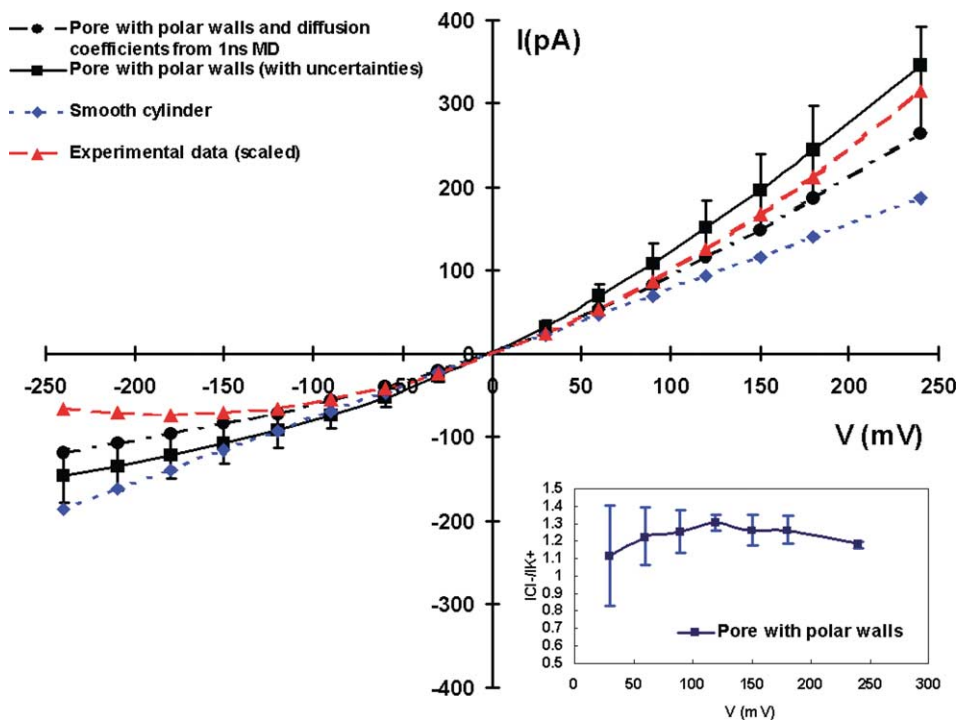


Figure 8. Current–voltage characteristics of the  $\alpha$ -hemolysin channel from MD-PNP calculations for a smooth cylindrical geometry (diamonds) and for a pore with polar walls (squares and circles). Experimental data points determined for a 0.1 M KCl concentration are also shown (triangles), after being linearly scaled to 1 M. The inset represents the ratio between the anion and the cation components of the ionic current for the pore with polar walls. Error bars in the ionic current values (squares) are determined from the standard deviations of the diffusion coefficients (table 3). The I–V curve calculated using the diffusion coefficients determined from 1 ns MD run is also shown (circles).

(inset of figure 8) seems related to the fact that, in the pore, anions have slightly larger diffusivities than cations (table 3).

The six determinations of diffusivities from repeated MD simulations contain one set of values (determined from the 1 ns MD run) for which the  $K^+$  diffusivity ( $0.38 \times 10^{-9} \text{ m}^2/\text{s}$ ) is larger than the  $Cl^-$  diffusivity ( $0.31 \times 10^{-9} \text{ m}^2/\text{s}$ ). To prove the slight anion selectivity of the channel the ionic current value and its component was calculated using the PNP model. Although the cation diffusivity is larger, the anion current component should dominate.

The I–V characteristic determined for this set of diffusion coefficients is also shown (circles in figure 8) and lies within the previously determined standard deviations. The ionic current calculated for an applied 120 mV potential difference is 114.8 pA. The corresponding conductance is 0.96 ns, again in good agreement with the experimental determinations. Although the cation diffusivity is larger than that of the anions, 51% of the total current ( $\sim 58.6 \text{ pA}$ ) is contributed by the anionic flow and 49% (56.2 pA) by the cation flow. From the same 1 ns MD trajectory, the values of  $0.22 \times 10^{-9} \text{ m}^2/\text{s}$  for  $K^+$  and  $0.18 \times 10^{-9} \text{ m}^2/\text{s}$  for  $Cl^-$  are determined for the pore stem selection. Correspondingly, the total ionic current drops by a factor of  $\sim 1.7$  ( $\sim 66.6 \text{ pA}$ ) and the anion (32.5 pA) and cation (34 pA) components scale by the same factor with the anionic component dominating. If one decreases the minimum radius of the pore at the constrictions to 6.25 Å,

value closer to the real channel constriction diameters, the total current becomes 108.9 pA, underestimating the experimental value by  $\sim 9\%$ . This is still a good prediction given the relative simplicity of the employed hybrid MD-PNP model. For the pore stem approximated by a smooth cylinder of radius 8.75 Å (no constricting blocks) the current is 132.9 pA. Thus, the geometric presence of the two constrictions is responsible for reducing the current by 21% of which  $\sim 7\%$  is due to  $C_2$  and  $\sim 16\%$  to  $C_1$  (table 6).

Indeed, the ionic currents should decrease more in the presence of the larger constriction  $C_1$  than that of  $C_2$ . The effect should sum up when both constrictions are

Table 6. Open channel ionic currents for  $\alpha$ -hemolysin corresponding to a 120 mV applied potential and 1 M KCl solution.

	I (pA)		
	Total	$K^+$	$Cl^-$
Smooth cylinder with two constrictions and fixed charges	114.8	56.2	58.6
Smooth cylinder	132.9	73.2	59.7
Smooth cylinder with constriction $C_2$	123.6	68.1	55.5
Smooth cylinder with constriction $C_1$	111.6	61.5	50.2
Smooth cylinder with two constrictions ( $C_1$ and $C_2$ )	104.9	57.8	47.2

The pore stem is approximated by a cylinder of radius 8.75 Å. At the two constrictions the radius is reduced to 6.75 Å. The diffusion coefficients of the two ionic species determined from 1 ns of MD are  $0.38 \times 10^{-9}$  and  $0.31 \times 10^{-9} \text{ m}^2/\text{s}$ , respectively.

present. In the absence of atomic charges, the contribution to the total current should also be larger for the cations than for the anions in direct proportionality with the 1 ns MD determined diffusion coefficients ( $0.38 \times 10^{-9} \text{ m}^2/\text{s}$  for  $\text{K}^+$  and  $0.31 \times 10^{-9} \text{ m}^2/\text{s}$  for  $\text{Cl}^-$ ). The values in Table VI are useful for a qualitative analysis of what determines the value of the ionic current when all the critical system parameters are included (constrictions and charges). As shown above, in bulk ionic solution the diffusion coefficient of  $\text{K}^+$  ions is larger than that of  $\text{Cl}^-$  ions. Inside a smooth cylindrical pore the diffusion coefficients will be scaled down to some value, however, without altering the hierarchy:  $\text{K}^+$  will still diffuse faster than  $\text{Cl}^-$  leading to a larger cationic versus anionic component. The presence of some geometrical constrictions may reduce the diffusion coefficients even more but would again only determine the absolute values of the ionic current and not reorder the anion and cation contributions. Constrictions are clearly reducing the ionic current. However, the pore specific surface chemistry is responsible for increasing the total current by disproportionately increasing the anion over the cation current contribution.

The electric field in the pore becomes distorted by the dielectric boundary and enhanced by the fixed charges (figure 9). In the absence of any fixed charges on the protein and for a simple cylindrical geometry that includes the two constriction blocks, the strength of the electric field across the channel induced by a membrane potential of 120 mV drops linearly. The geometry is only responsible for curving the field lines. For both direct and reverse potential ( $-120 \text{ mV}$ ), with the addition of

charges, local variations inside the channel around the two constrictions are observed. The strength of the electric field increases sharply around the edges of the constriction blocks and decreases in some regions of the pore along the pore walls. The potentials inside the molecule are larger in magnitude than the applied potential ranging from  $-420$  to  $380 \text{ mV}$  (figure 9). The more saturated red and blue regions (figure 9; top) are correlated with the position of the amino acids on the pore stem as indicated in figure 5 (the representation in the PNP model is rotated by  $180^\circ$ ). The dipole associated to the pore stem enhances the electrical potential values in the region with  $0 \text{ mV}$ -applied potential, and reduces the potential values in the  $120 \text{ mV}$ -applied potential (figure 9; bottom).

It is known that for ion channels strongly selective towards one of the permeating ion species, the passage of anions may depend on the presence of cations and vice versa, especially in constricted regions [28]. Such ion-ion pairing (observed to a less extent in bulk solution) increases with concentration, and results in the reduction of the effective ion diffusion coefficients. Within the pore boundary, such correlations become important, leading to concentration build up several times larger than the concentration in the bulk solution. For example, for OmpF, both  $\text{K}^+$  and  $\text{Cl}^-$  concentrations raise to more than  $5 \text{ M}$  in the constriction zone while the molarity in the bulk solution is only  $1 \text{ M}$  [28]. If such effects are not considered by including a concentration dependent diffusion coefficient or an empirical scaling factor of the ions diffusion constants, the PNP calculations overestimate the conductance and the ionic current values (for OmpF this amounts to about 20%).

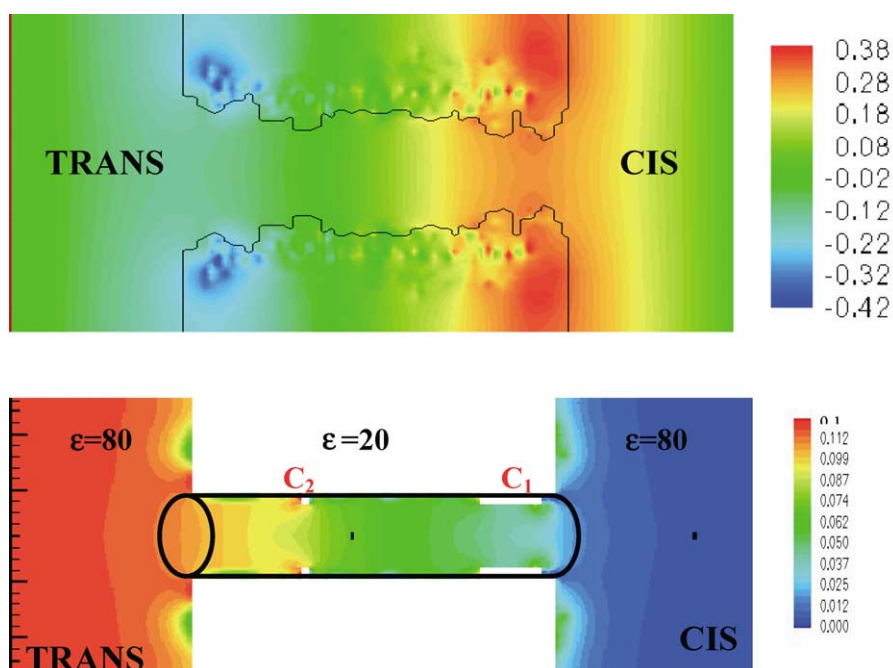


Figure 9. Schematic view of the  $\alpha$ -hemolysin protein stem used in the PNP model. Red indicates regions of high potential and blue indicates low potential. The applied potential is  $+0 \text{ mV}$  on the right side and  $+120 \text{ mV}$  on the left side (bottom). The potentials inside the molecule are larger in magnitude than the applied potential ranging from  $-420$  to  $380 \text{ mV}$  (top). The scales on the right are in units of Volts.

So far, our PNP model does not include such correction factors. Experimental evidence [17] shows that the  $\alpha$ -hemolysin channel is only slightly anion selective. The smallest constriction is  $\sim 12$  Å (about 25% larger than the constriction of OmpF) thus, the effect of a concentration built up might have less impact on the conductance properties. However, more insight into the presence of such effects in the  $\alpha$ -hemolysin pore is required.

### Pore selectivity

The inset in figure 8 shows that the ratio of anionic versus cationic current components is about  $\sim 1.2$ . This value is in agreement with the experimental determination of the ratio of transport coefficients of  $\text{Cl}^-$  versus  $\text{K}^+$  [17]. Once again this demonstrates that the channel has slight anion selectivity, meaning that the channel is open to and will transport both ion types, however, with a slight preference for  $\text{Cl}^-$  versus  $\text{K}^+$ .

The best binding energies of the  $\text{K}^+$  and  $\text{Cl}^-$  ions with the “reduced” representation of the  $\alpha$ -hemolysin pore are calculated using the GRID (Molecular Discovery Inc.) software. Figure 10 (top) shows the distribution of the best binding sites for  $\text{K}^+$  (left) and  $\text{Cl}^-$  ions (right). Inside the channel, the *cis* and *trans* ends offer favorable binding sites for the positive potassium ions with the best overall binding energy of  $-40$  kcal/mol. For chloride ions, however, the best binding sites are distributed around the  $\text{C}_1$  constriction with a much smaller overall energy of

only  $-9$  kcal/mol. These distributions are correlated also with the electrostatic potential lines in figure 9 (top).

The slight anion selectivity most probably originates from the fact that the LYS amino acid that has a basic character (thus, being attractive to anions) defines the smallest radius for constriction  $\text{C}_1$ . Thus,  $\text{Cl}^-$  passage (and to a lesser extent that of  $\text{K}^+$ ) is favored through the narrowest part of the channel.

The chemistry of the second constriction ( $\text{C}_2$ ) seems to be less important for ions than for water. The LEU amino acid that forms  $\text{C}_2$  is hydrophobic. From both, binding sites calculations and MD simulations (figure 10), the distribution of water molecules exhibits discontinuities around the two constrictions ( $\text{C}_1$  includes MET that is a hydrophobic amino acid), due to geometry and local chemistry. For comparison, the best binding energy for water in the channel is  $-16$  kcal/mol.

### Conclusions

A hybrid MD PNP model is employed to study the conductance properties of the  $\alpha$ -hemolysin channel solvated in a 1 M KCl solution. The diffusion coefficients of the  $\text{K}^+$  and  $\text{Cl}^-$  ions are calculated from full atomistic MD simulations. It is found that the diffusion coefficients of the ions within the channel are reduced by a factor of 5–7 relative to bulk solution, consistent with previous studies of ions within various model channels [15,27].

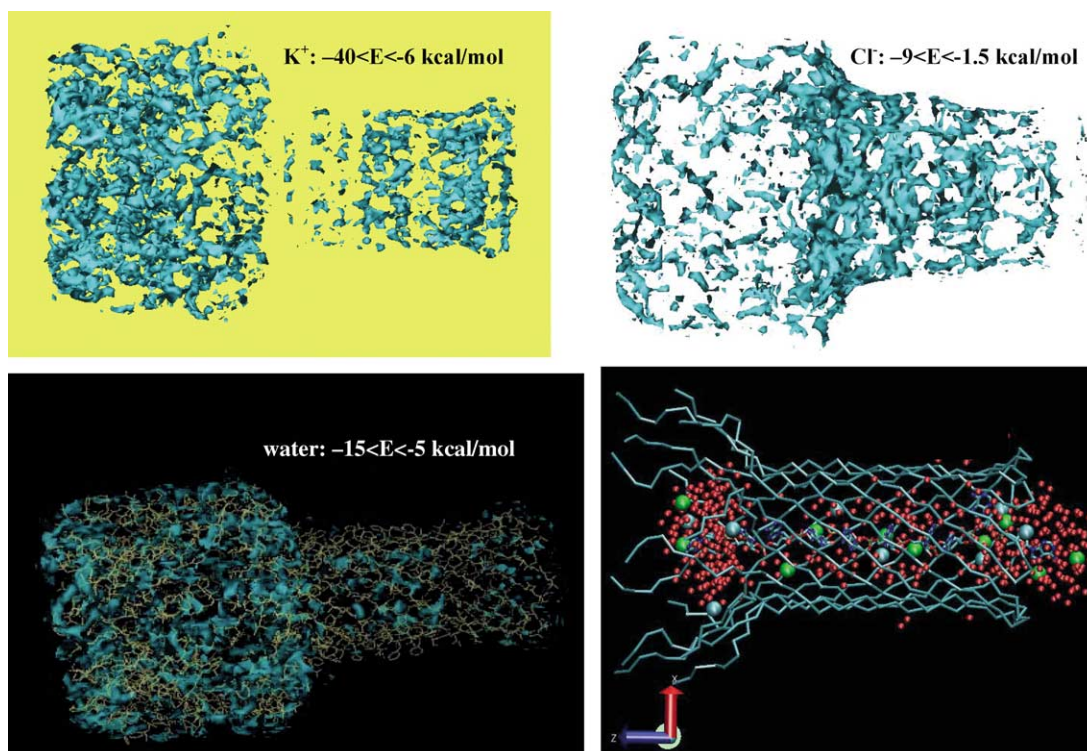


Figure 10. Binding energies inside the  $\alpha$  hemolysin pore for  $\text{K}^+$  (top left),  $\text{Cl}^-$  (top right) and water (bottom left). The blue colored regions indicate the distribution of the binding sites that have energy within the range indicated in the captions. For comparison (bottom right), the distribution from MD simulations of solvent molecules in the van der Waals representation inside the pore stem is shown (water molecules in red,  $\text{K}^+$  in light green and  $\text{Cl}^-$  in blue).

At 1 M concentration the pore channel only includes ~30–34 ion pairs leading to relatively poor statistics for the analysis of the diffusion process. The small number of ions used to calculate the time variation of the mean square displacement will lead to a noisy profile and to deviations from linearity. This is reflected in the statistical variations (17–45%) of the standard deviations of the ionic diffusivities. The axial and radial components of the pore-ions diffusivities are determined with even lower precision. However, there seems to be a trend in the values indicating a dominant axial movement of the ions (the radial component of the motion is hindered) that could be associated with the presence of the pore strong dipole field. The variation of ionic diffusivities with the applied voltage (30–240 mV) lies within the statistics determined from repeated MD runs. Thus, one may conclude that the ion diffusivities are independent on the applied potential which, based on the assumption of the fluctuation–dissipation theory, is to be expected.

Although in the PNP simulations only the stem of the pore is included, approximated by a smooth cylinder ( $R = 8.75 \text{ \AA}$ ) with two constriction blocks ( $R = 6.75 \text{ \AA}$ ), the calculated conductance properties of the channel are, within statistics, in very good agreement with the experimental current–voltage profiles. The distribution of atomic charges characteristic to the  $\alpha$ -hemolysin pore is responsible not only for the rectifying behavior of the channel but also for its slight anion selectivity. The anions are the major contributors to the total ionic current, regardless of the relative values of the anion and cation diffusivities.

The beauty of the present hybrid MD-PNP model is that it accounts for the key parameters (diffusion coefficients and channel specific chemistry) responsible for both the rectifying behavior of the channel and its “slight” anion selectivity without being computationally too expensive or difficult to use.

In the future, this hybrid model will be used to account for the presence of polynucleotides inside the protein channel in an attempt to predict blockade durations for various translocating polymers. The model will be also used to calculate ionic currents for both organic and inorganic pores in the presence of pore-specific surface chemistries. Results could be used in the experimental design of a solid-state nanopore with single nucleotide resolution for sequencing purposes.

## Acknowledgements

The present work was supported by DARPA and NASA Ames Research Center. I. Cozmuta was supported by NASA contract NAS2-99092 to Eloret and acknowledges the ASN system administrators and the NAS support for technical assistance with NASA computers and the Amber, VMD and NAMD lists for software related support. The authors would like to thank M. Brock, T.R. Govindan, D. Hash and R. Jaffe for their comments on the manuscript.

## References

- [1] L. Song, *et al.* Structure of staphylococcal  $\alpha$ -hemolysin, a heptameric transmembrane pore. *Science*, **74**, 1859 (1996).
- [2] J.J. Kasianowicz, *et al.* Characterization of individual polynucleotide molecules using a membrane channel. *Proc. Natl Acad. Sci. USA*, **93**, 13770 (1996).
- [3] D.W. Deamer, M. Akeson. Nanopores and nucleic acids: prospects for ultrarapid sequencing. *Trends Biotechnol.*, **18**, 147 (2000).
- [4] M. Akeson, *et al.* Microsecond time-scale discrimination among polycytidylic acid, polyadenylic acid, and polyuridylic acid as homopolymers or as segments within single RNA molecules. *Biophys. J.*, **77**, 3227 (1999).
- [5] D. Branton, J. Golovchenko. Adapting to nanoscale events. *Nature*, **398**, 660 (1999).
- [6] D.G. Levitt. Modeling of ion channels. *J. Gen. Phys.*, **113**, 789 (1999).
- [7] D.K. Lubensky, D.R. Nelson. Driven polymer translocation through a narrow pore. *Biophys. J.*, **77**, 1824 (1999).
- [8] D.P. Tieleman, *et al.* Simulation approaches to ion channel structure–function relationship. *Qrtly. Rev. Biophys.*, **34**, 473 (2001).
- [9] T. vd Straaten, *et al.* Combining computational chemistry and computational electronics to understand protein ion channels, *Proc. Second. Conf. Comp. Nanosc. and Nanotech.*, Puerto Rico, USA, April (2002).
- [10] U. Hollerbach, *et al.* Predicting function from structure using the Poisson–Nernst–Planck equations: sodium current in the gramicidin A channel. *Langmuir*, **16**, 5509 (2000).
- [11] L. Kale, *et al.* NAMD2: Greater scalability for parallel molecular dynamics. *J. Comp. Phys.*, **151**, 283 (1999).
- [12] W.D. Cornell, *et al.* A second generation force field for the simulation of proteins, nucleic acids and organic molecules. *J. Am. Chem. Soc.*, **117**, 5179 (1995).
- [13] D.A. Pearlman, *et al.* AMBER, a package of computer programs for applying molecular dynamics and free energy calculations to simulate the structural and energetic properties of molecules. *Comp. Phys. Commun.*, **91**, 1 (1995).
- [14] W. Humphrey, A. Dalke, K. Shulten. VMD-visual molecular dynamics. *J. Mol. Graphics*, **14**, 33 (1996).
- [15] G.R. Smith, M.S.P. Sansom. Effective diffusion coefficients of  $\text{K}^+$  and  $\text{Cl}^-$  ions in ion channel models. *Biophys. Chem.*, **79**, 129 (1999).
- [16] H.C. Andersen. Rattle: a ‘velocity’ version of the shake algorithm for molecular dynamics calculations. *J. Comp. Phys.*, **52**, 24 (1983).
- [17] G. Menestrina. Ionic channels formed by *Staphylococcus aureus*  $\alpha$ -toxin: voltage-dependent inhibition by divalent and trivalent cations. *J. Membr. Biol.*, **90**, 177 (1986).
- [18] L. Gu, H. Bayley. Interaction of the noncovalent molecular adapter,  $\beta$ -cyclodextrin, with the Staphylococcal  $\alpha$ -hemolysin pore. *Biophys. J.*, **79**, 1967 (2001).
- [19] W. Vercoutere, *et al.* Rapid discrimination among individual DNA hairpin molecules at single-nucleotide resolution using an ion channel. *Nature Biotechnol.*, **19**, 248 (2001).
- [20] F.C. Bernstein, *et al.* The Protein Data Bank: a computer based archival file for macromolecular structures. *J. Mol. Biol.*, **112**, 535 (1977).
- [21] L. Movileanu, H. Bayley. Partitioning of a polymer into a nanoscopic protein pore obeys a simple scaling law. *PNAS*, **98**, 10137 (2001).
- [22] M.L. Connolly. Analytical molecular surface calculation. *J. Appl. Crystallogr.*, **16**, 548 (1983).
- [23] H.J.C. Berendsen, J.R. Grigera, T.P. Straatsma. The missing term in effective pair potentials. *J. Phys. Chem.*, **91**, 6269 (1987).
- [24] R.J. Mashl, *et al.* Hierarchical approach to predicting permeation in ion channels. *Biophys. J.*, **81**, 2473 (2001).
- [25] G.R. Smith, M.S.P. Sansom. Dynamic properties of  $\text{Na}^+$  ions in models of ion channels: a molecular dynamics study. *Biophys. J.*, **75**, 2767 (1998).
- [26] D.W. Deamer, M.A. Akeson, and J.J. Kasianowicz. Mechanism of ionic current blockades during polymer transport through pores with nanometer dimensions, *NATO Advanced Research Workshop*, Bikal, Hungary, June 20–25 (1999).
- [27] P.S. Crozier, *et al.* Model channel ion currents in  $\text{NaCl}$ -SPC/E solution with applied field molecular dynamics. *Biophys. J.*, **81**, 3077 (2001).

- [28] W. Im, B. Roux. Ion permeation and selectivity of OmpF Porin: a theoretical study based on Molecular Dynamics, Brownian Dynamics and Continuum Electrodiffusion Theory. *J. Mol. Biol.*, **322**, 851 (2002).
- [29] P. Atkins. *Physical Chemistry*, 6th Ed., W.H. Freeman and Co., New York (2000).
- [30] S. Kuyucak, O.S. Andersen, S.H. Chung. Models of permeation in ion channels. *Rep. Prog. Phys.*, **64**, 1427 (2001).
- [31] D. Beglow, B. Roux. Finite representation of an infinite bulk system: solvent boundary potential for computer simulations. *J. Chem. Phys.*, **100**, 9050 (1994).
- [32] P. Mark, L. Nilsson. Structure and dynamics of the TIP3P, SPC and SPC/E water models at 298 K. *J. Phys. Chem.*, **105**, 9954 (2001).
- [33] A.H. Narten, H.A. Levy. Liquid water: molecular correlation functions from X-ray diffraction. *J. Chem. Phys.*, **55**, 2263 (1971).
- [34] W.F. van Gunsteren, H.J.C. Berendsen. Algorithms for macromolecular dynamics and constraint dynamics. *Mol. Phys.*, **34**, 1311 (1977).
- [35] D. Bose, T.R. Govindan, M. Meyyappan. Modeling of a helicon plasma source. *IEEE Plasma Sci.*, **3**, 653 (2002).
- [36] M. Jardat, O. Bernard, P. Turq. Transport coefficients of electrolyte solutions from smart Brownian dynamics simulations. *J. Chem. Phys.*, **110**, 7993 (1999).
- [37] S. Chowduri, A. Chandra. Molecular dynamics simulations of aqueous NaCl and KCl solutions: effects of ion concentration on the single-particle, pair, and collective dynamical properties of ions and water molecules. *J. Chem. Phys.*, **115**, 3732 (2001).
- [38] J.F. Dufreche, *et al.* Ionic self-diffusion in concentrated aqueous electrolyte solutions. *Phys. Rev. Lett.*, **88** (2002).
- [39] J.F. Chambers, J.M. Stokes, R.H. Stokes. Conductances of concentrated aqueous sodium and potassium chloride solutions at 25°C. *J. Phys. Chem.*, **60**, 985 (1956).
- [40] T. Schlick, *et al.* Algorithmic challenges in computational molecular biophysics. *J. Comput. Phys.*, **151**, 9 (1999).
- [41] T. Darden, D. York, L. Pedersen. Particle mesh Ewald. An  $N \log(N)$  method for Ewald sums in large systems. *J. Chem. Phys.*, **98**, 10089 (1993).
- [42] I. Cozmuta, J.T. O’Keeffe, V. Stolz, Towards an MD simulation of ion currents in the alpha hemolysin channel. IEEE-Nano Conference, San Francisco, CA, August (2003).
- [43] T. Bastug, S. Kuyucak. Role of the dielectric constants of membrane proteins and channel water in ion permeation. *Biophys. J.*, **84**, 2871 (2003).
- [44] W. Rocchia, E. Alexov, B. Honig. Extending the applicability of the nonlinear Poisson–Boltzmann equation: multiple dielectric constants and multivalent ions. *J. Phys. Chem. B*, **105**, 6507 (2001).
- [45] B. Eisenberg. Ionic channels in biological membranes: natural nanotubes. *Acc. Chem. Res.*, **31**, 117 (1998).
- [46] M.P. Allen, D.J. Tildesley. *Computer Simulations of Liquids*, Oxford Science Publications/Clarendon Press, Oxford (1997).
- [47] D. Chen, J. Lear, B. Eisenberg. Permeation through an open channel: Poisson–Nernst–Planck theory of a synthetic ionic channel. *Biophys. J.*, **72**, 97 (1997).
- [48] M.G. Kurnikova, *et al.* A lattice relaxation algorithm for 3D Poisson–Nernst–Planck theory with application to ion transport through the gramicidin A channel. *Biophys. J.*, **76**, 642 (1999).

Dear Author,

During the preparation of your manuscript for typesetting some questions have arisen. These are listed below. Please check your typeset proof carefully and mark any corrections in the margin of the proof or compile them as a separate list. This form should then be returned with your marked proof/list of corrections to Aldent Multimedia.

#### Disk use

In some instances we may be unable to process the electronic file of your article and/or artwork. In that case we have, for efficiency reasons, proceeded by using the hard copy of your manuscript. If this is the case the reasons are indicated below:

- ☐ Disk damaged    ☐ Incompatible file format    ☐ LaTeX file for non-LaTeX journal  
☐ Virus infected    ☐ Discrepancies between electronic file and (peer-reviewed, therefore definitive) hard copy.  
☐ Other: .....

We have proceeded as follows:

- ☐ Manuscript scanned    ☐ Manuscript keyed in    ☐ Artwork scanned  
☐ Files only partly used (parts processed differently: )

#### Bibliography

If discrepancies were noted between the literature list and the text references, the following may apply:

- ☐ The references listed below were noted in the text but appear to be missing from your literature list. Please complete the list or remove the references from the text.
- ☒ *Uncited references*: This section comprises references which occur in the reference list but not in the body of the text. Please position each reference in the text or, alternatively, delete it. Any reference not dealt with will be retained in this section.

Manuscript page/line	Details required	Author's Response
	Kindly provide the full article history.  As table 3 was not provided Tables 4 to 7 has been changed to Tables 3 to 6 for continuity. Kindly check.  Author, this reference is not cited in the text. Please add or delete from reference list. Reference 7: [7].	